Automatic Fast and Robust Technique to Refine Extracted SIFT Key Points for Remote Sensing Images

Hayder Dibs[1,2], Shattri Mansor[2], Noordin Ahmad[3], Biswajeet Pradhan[2] and Nadhir Al-Ansari[4]

1. Hydraulic Structures Department, Faculty of Water Resources Engineering, Al-Qasim Green University, Al-Qasim 964, Babylon, Iraq

2. Department of Civil Engineering, Faculty of Engineering, Geospatial Information Science Research Centre, University Putra Malaysia, Level 6, Tower Block, Serdang 43400, Darul Ehsan, Selangor, Malaysia

3. National Space Agency Malaysia (ANGKASA), Kementerian Sains, Teknologi dan Inovasi, Pusat Angkasa Negara, Lot 2233, Jalan Turi, Kg. Sg. Lang, Banting Selangor 42700, Malaysia

4. Department of Civil Environmental and Natural Resources Engineering, Lulea University of Technology, Lulea 97187, Sweden

Abstract: The scale-invariant feature transform (SIFT) ability to automatic control points (CPs) extraction is very well known on remote sensing images, however, its result inaccurate and sometimes has incorrect matching from generating a small number of false CPs pairs, their matching has high false alarm. This paper presents a method containing a modification to improve the performance of the SIFT CPs matching by applying sum of absolute difference (SAD) in different manner for the new optical satellite generation called near-equatorial orbit satellite (NEqO) and multi-sensor images. The proposed method leads to improving CPs matching with a significantly higher rate of correct matches. The data in this study were obtained from the RazakSAT satellite covering the Kuala Lumpur-Pekan area. The proposed method consists of three parts: (1) applying the SIFT to extract CPs automatically, (2) refining CPs matching by SAD algorithm with empirical threshold, and (3) evaluating the refined CPs scenario by comparing the result of the original SIFT with that of the proposed method. The result indicates an accurate and precise performance of the model, which showed the effectiveness and robustness of the proposed approach.

Key words: Automatic extraction of ground control point, sum of absolute difference, near-equatorial satellite, multi-sensor, modified SIFT.

1. Introduction

Extracting ground control points (GCPs) from remotely sensed imagery is an important step for different types of remote sensing applications. Thus, it received considerable attention [1, 2]. Therefore, a robust and flexible technique is necessary to extract the GCPs automatically, and then refine and improve the extracted GCPs automatically. The refined GCPs should then be used in determining transformation coefficients in different types of remote sensing applications. SIFT algorithm is used for this study, it is one of the most effective algorithms that have been used to extract the control points from images automatically [3, 4], however, applying scale-invariant feature transform (SIFT) for remote sensing imagery either performs poorly or fails completely and will produce false CPs which lead to making error in CPs matching. Therefore, matched CPs pairs correctness is important. It is very common to get location error for SIFT CPs [4-8]. Finding an accurate method of refining the GCP quality becomes a difficult task that prevents the broad development of automatic GCP extraction. The GCPs collected from images are selected by visual interpretation and selecting GCPs from the field is not economically viable. It requires considerable time and labor, particularly in hilly and/or mountainous areas that are

Corresponding author: Nadhir A. Al-Ansari, professor, research fields: water resources and environment.

difficult to reach. Despite preparations, this procedure can still obtain inaccurate results, and sometimes the collected GCPs are extremely poor, especially if they are obtained over a large area [9-15]. The captured remotely sensed imagery especially from near-equatorial satellite and multi-sensor contains nonlinear geometric distortions [16]. This type of errors is non-systematic, and overcoming such errors is impossible to collect GCPs by conventional techniques because of the differences in altitude (sensor and topographic terrain), attitude (pitch, roll, and yaw), capturing time, illumination, viewing points, sun zenith and azimuth, and sensor zenith and azimuth during image capture [16-28]. So, it is necessary to robust and automatic techniques to select the GCPs for remote sensing images.

Over the past decades, numerous studies proposed many types of local feature extraction techniques. The SIFT algorithm, which was proposed by Lowe [3, 4]. It is suitable and effective in extracting CPs from remotely sensed images. These CPs are robust to changes in image scaling, skewing, illumination, and rotation with changes in viewpoints [3, 4]. SIFT has been applied to different applications in computer vision, remote sensing, object recognition, medicine, and robotics [29-37]. Modified SIFT algorithms have been widely employed in synthetic aperture radar (SAR) imagery [3, 38]. Chureesampant and Susaki [37] compared the SIFT-dealing performance of SAR images in different polarizations. Wang et al. [39] modified SIFT and called it bilateral filter SIFT (BFSIFT), which is used in the pyramid construct instead of the Gaussian filter.

The extraction of CPs for remote sensing images by employing the SIFT algorithm has also been improved. For example, Shragai et al. [40] used the SIFT algorithm to extract CPs from aerial imagery; it provided good results. Wessel et al. [41] modified a technique to extract GCPs for near-real-time SAR images and integrated it with the digital elevation model (DEM). Liu and Yu [6] used the SIFT

algorithm to match the sensed and reference images after performing edge extraction on SAR images. Liu et al. [42] applied the SIFT-based automatic CPs extraction for radar images. For this work we should get knowledge with challenges of SIFT algorithm with remote sensing images and how to refine image matching by using sum of absolute difference.

1.1 SIFT-Challenges with Remote Sensing Images

Remote sensing images such as multi-sensor and near equatorial orbit satellite (NEqO) capture the imagery at different times and a wide range of frequencies, one of the main difficulties with remote sensing images is that the intensity variation is not linear and in most cases the relationship is not even a one-to-one relationship [43]. Images captured at different frequencies have a different kind of response. Several studies [8, 44] have shown that employing SIFT directly into different remote sensing imagery either fails completely and/or performs poorly and will generate false CPs which lead to making error in CPs matching. So, correctness of the matched key point pairs is important, it is very common to have position error for SIFT key point [4, 6, 8, 30].

1.2 Refining of Image Matching by Using Sum of Absolute Difference

Using the extracted SIFT CPs led to numerous false and incorrect matches. It increased errors in image matching and negatively affected the application of these images in remote sensing application [43, 45, 46]. Using observation geometry by wavelets is highly robust when large image differences.

In this study, the generated SIFT CPs are refined by using the sum of absolute difference (SAD) algorithm. Matching is simple and easy to implement. It can determine the relationship between the image windows in both reference and slave images. The SAD algorithm [47, 48] is adopted to refine the generated SIFT CPs. The process is performed by removing the incorrectly matched CPs when the SIFT

algorithm is run. SAD functions based on the concept of conventional approach, which measures the similarity in intensity between the reference and slave images by calculating the absolute differences between each CP in the image window and the corresponding CP in the search. Thereafter, all these differences should be integrated so that the similarity between two imageries is identified. Empirical threshold determines the removal of false CPs pairs that have matching errors.

Several studies employed the SAD algorithm in their applications, such as object recognition, motion estimation, and video compression [32, 49-55]. Generally, refining the CPs is an important step in obtaining high-quality CPs because CPs candidates are identified in this step [11]. SAD can be expressed as follows:

$$SAD = \sum \sum |A(x,y) - B(x,y)| \qquad (1)$$

where A and B are blocks, and x and y are the pixel indices of matrices A and B.

This study aims to present a new technique of automatically refining the extracted SIFT CPs for remotely sensed images. This approach is performed by removing the bad generated SIFT CPs using the SAD algorithm with empirical threshold. The proposed method is called refined SIFT CPs (R-SIFT).

In this paper, a new modification technique of SIFT CPs matching is proposed to remove the false CPs pairs that have a fake matching by using SAD algorithm in different manners which have not been used before and then obtain a new and accurate SIFT CPs to use for solving transformation function parameters for remote sensing applications such as registration and geometric correction models. This method called R-SIFT, using the R-SIFT in applications of remote sensing will reduce the processing time, and increase the accuracy level of remote sensing applications from removing the false CPs, no need to manual selecting of CPs.

Recommendations are made in the context of image registration, band-to-band co-registration, image fusion, change detection, target detection, and geometric correction of multi-sensor and near-equatorial satellite images, which can be used with pattern reorganization, robotics, and computer vision.

2. Method of Refining Extracted SIFT GCPs

A new methodology to refine and improve the generated SIFT CPs automatically, which is called R-SIFT, is introduced in this study. This methodology is described in Fig. 1. The proposed approach starts by selecting the reference and slave images, and then converting each of them into grayscale. Thereafter, image compression is performed on both images. Next, the SIFT algorithm is applied to generate CPs automatically. Finally, the generated CPs are refined by using the SAD algorithm, which measures and compares the correlation similarity in brightness values (intensities) between the CPs in the reference and slave images to avoid obtaining bad CPs and errors in image matching. Evaluations of the R-SIFT method are performed by comparing the result of the R-SIFT with that of the original SIFT.

2.1 Dataset

The remotely sensed image used in this study is obtained from the near-equatorial satellite Malaysian RazakSAT over the study area located between 102°19′55″ E-103°27′08″ E and 02°50′36″ N-02°39′22″ N, which is over Kuala Lumpur-Pekan, Malaysia. The satellite image represents the area that is approximately 2,000 km², and the image acquisition date is August 1, 2009. The RazakSAT image has four multispectral bands (green, red, blue, and near infrared), and one has a panchromatic band. Fig. 2 shows the location of the study area.

2.2 Selection of Reference Image

One of the difficulties encountered in this study is selecting the reference image because only one
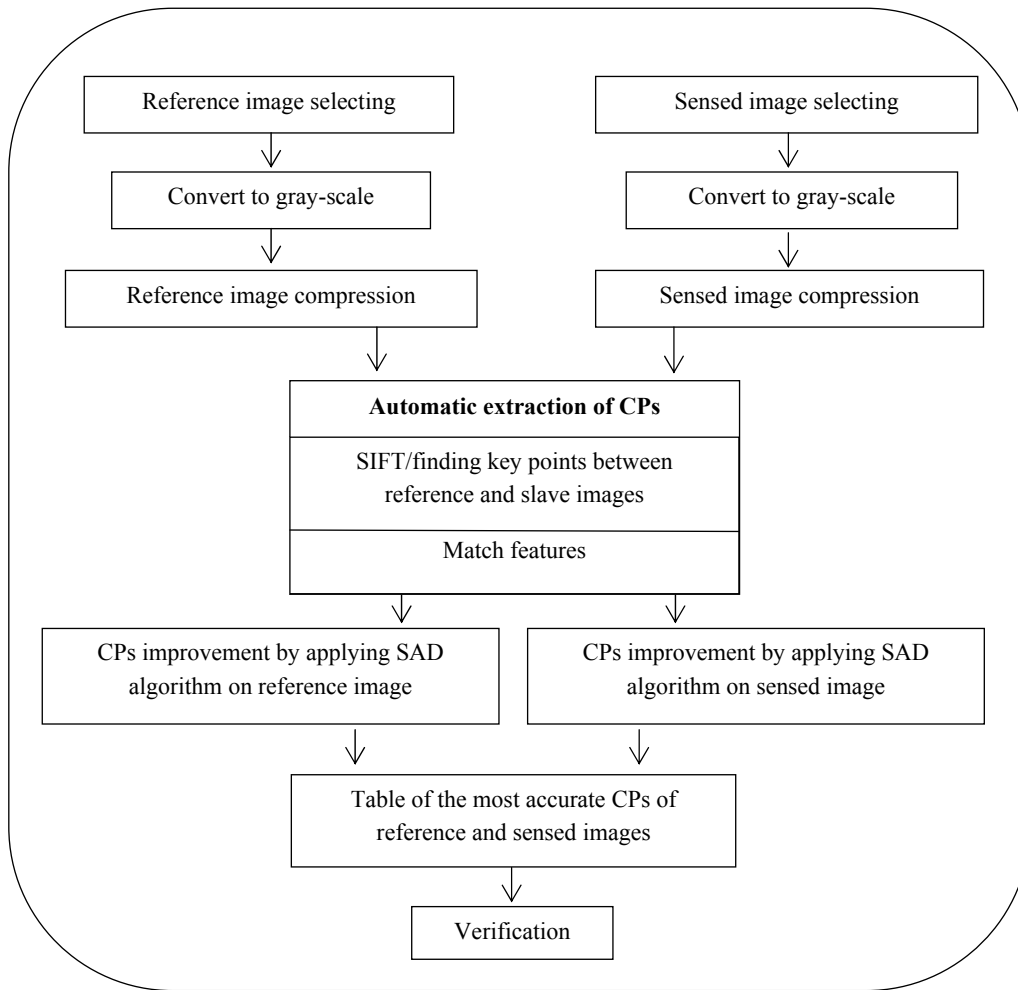
Fig. 1 Process flow of the R-SIFT method.

satellite image is available. Fortunately, the bands of this image have high distortion (non-linear), which is perfect in this study. Each band of the image is considered as an individual image, and these four bands are involved in implementing the R-SIFT method. The image used in this study is related to the near-equatorial satellite. All the bands in the image have a similar amount of noise, skewness, stretching, and rotation. Slight differences were observed in the study area [11, 56-58]. However, the green band exhibits fewer defects and is suitable as the reference image, and the rest of the bands can be considered as slave imagery.

2.3 Gray-Scale Conversion

A grey-scale-level image demonstrates a matrix of imagery, and each value (pixel value) in the matrix is represented in gray scale based on image depth [10, 14, 59]. The first stage of the proposed method involves converting the imagery to gray-scale level by using the Matlab software. The mathematical expression that has been used is:

$$Gray = \frac{R + G + B}{3} \qquad (2)$$

where R, G and B are the bands of coloured image red, green and blue respectively.

2.4 Image Compression

Image compression is the science of reducing the amount of data required to represent an image, it is also the reduction of data that encode the original image to few bits. Image compression is used in this study to
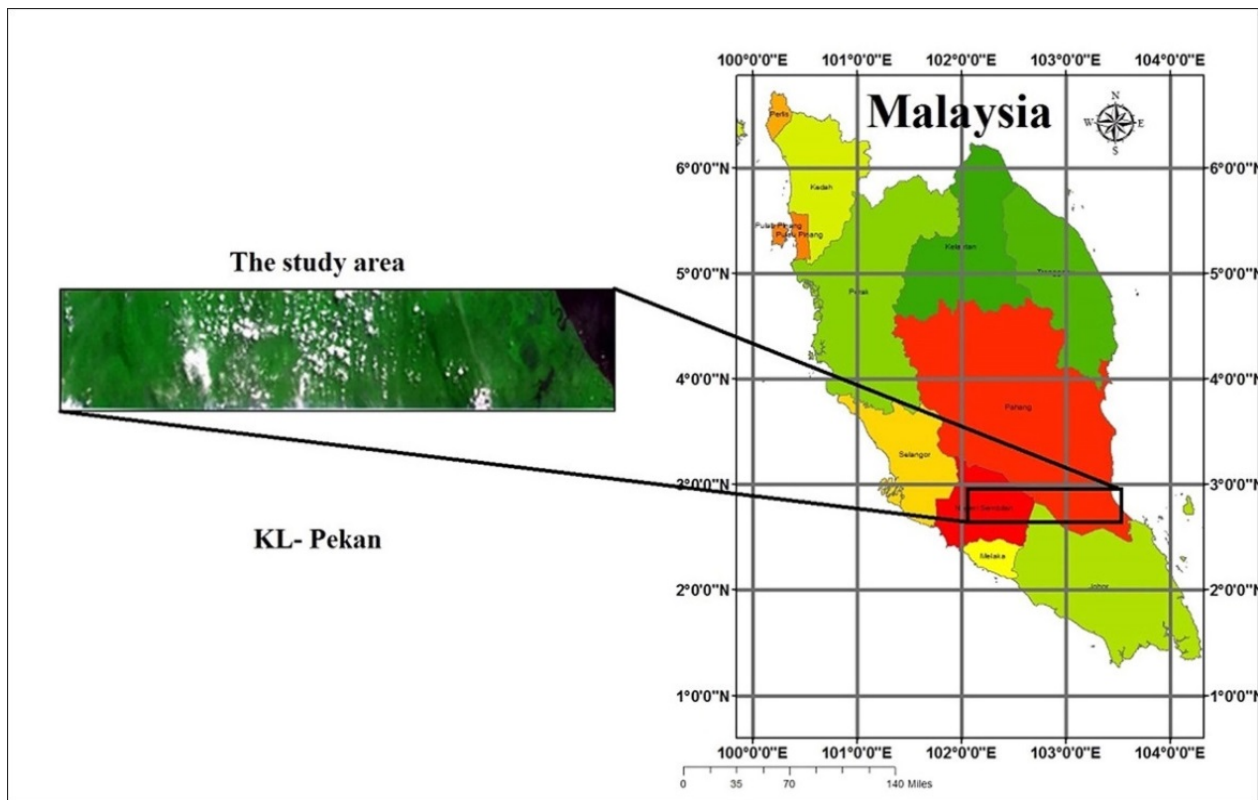
Fig. 2   Location of the study area.

reduce the processing time and storage requirements as much as possible [10, 59, 60]. In this study, the image is converted into JPEG form through image compression to minimize its size [59, 61], the processing time before performing image compression was two days, but after the image compression the processing time reduced dramatically to become two minutes.

2.5 Automatic GCP Extraction Procedure

The automatic GCP extraction is performed by using the SIFT algorithm, which was introduced by Lowe [3, 4]. An outline of the pertinent points of the SIFT algorithm can be obtained by following these steps:

(1) scale-space extrema detection;

(2) key point localization;

(3) orientation assignment;

(4) key point descriptor.

The candidate key points are extracted by employing Lowe's SIFT algorithm. A large number of candidate key points are extracted, which contain many false matches [43-46]. The refinement strategies described in Sections 1.2 and 3 are used to remove.

3. Results and Discussion

The proposed method mainly aims to automatically refine and improve the extract SIFT CPs by using the SAD algorithm through refining the feature matching of SIFT algorithm. The SAD algorithm is used in different remote sensing applications. The SIFT algorithm was not created for imagery captured from different viewing points, such as multi-sensor and near-equatorial images, as previously indicated in Section 1. One of the main difficulties of the SIFT algorithm with remote sensing images is that the intensity variation in each pixel of the image does not have a linear relationship [43, 45]. Thus, the SIFT algorithm produces imprecise and inaccurate CPs for processing multi-sensor and near-equatorial satellite

images. When researchers apply these CPs, the geometric distortion in the remotely sensed images decreases and the accuracy level decreases [43, 46, 54]. Fig. 3a, shows the false extracted SIFT CPs that have errors in matching, such as those between locations 1, 2 and 3, 4. This error is related to the weakness of the SIFT algorithm with remote sensing images, as previously indicated. Therefore, refining the extracted CPs of SIFT is necessary. In this study, the SAD algorithm is used to refine the extracted SIFT CPs, in way different from previous studies, all the researchers apply the SAD algorithm in processing the entire reference and sensed images to identify the similarity matrix based on area correlation [19, 54, 62]. If this process is applied to find the similarity matrix for remotely sensed images, particularly with remote sensing imagery such as multi-sensor and/or near-equatorial satellite images, the extracted GCPs from SIFT will have false CPs leading to generating error in CPs matching. Add to that, SAD fails completely with images that have highly distortion such as multi-sensor imagery [52, 53, 55]. In other words, SAD cannot identify the correlated CPs because of the highly non-linear distortion and differences in intensities between the CPs in the sensed image and corresponding CPs in the reference image. SAD functions work well when minimal difference is observed between the two images [53, 55]. Involving the entire image in the SAD functions better with medical and computer vision applications than with satellite images because minimal difference is observed in illumination. No atmospheric effects or different viewing points are observed with this type of images [63, 64].

In this study, to overcome with the weakness of both SIFT and SAD with this kind of images, we propose a method that can overcome these problems as follows:

(1) The CPs should be automatically extracted by SIFT.

(2) The reference, sensed images and the image coordinates of the extracted SIFT CPs of both images should be entered in the SAD algorithm.

(3) Run SAD algorithm to measure the similarity in intensity between just the areas around the CPs of the sensed image and the correspondence CPs in the reference image, and remove the false CPs matches by using the empirical threshold.

The significance of using SAD for this study is by applying the CPs coordinates. The correlation by SAD between both images will be limited by using the location of this CPs. Following this procedure prevents the SAD from exploring the entire reference image to search for other correlated CPs to CPs of sensed image that have similar SAD values but not similar locations. Based on this process and empirical threshold the algorithm automatically removes the biased CPs and obtains the most precise and accurate ones. Implementing SAD in this manner enables analysts to obtain the most precise and accurate CPs that can be used in remote sensing applications. It also reduces the cost and time required in collecting precise CPs, which is the significance of using SAD. Fig. 3b, illustrates the successive matching after applying the SAD approach.

The result was obtained by empirically selecting the threshold. A value that was not extremely high or extremely small in between was selected to obtain a good number of CPs [52, 65]. The perfect frame size and threshold value for this study based on experimental results and the data used were 3 × 3 and 250, respectively, to remove the false CPs of SIFT. Tables 1-3 show the results of applying SIFT and SAD algorithms by using different threshold values and frame sizes for all images. The processing was performed in a Matlab environment.

Figs. 4 and 5 also illustrate that the SIFT algorithm is applied between the green image and each of the blue and near-infrared images, respectively. The extracted CPs are then refined by using the proposed R-SIFT. The number of CPs decrease after the false SIFT CPs are removed.
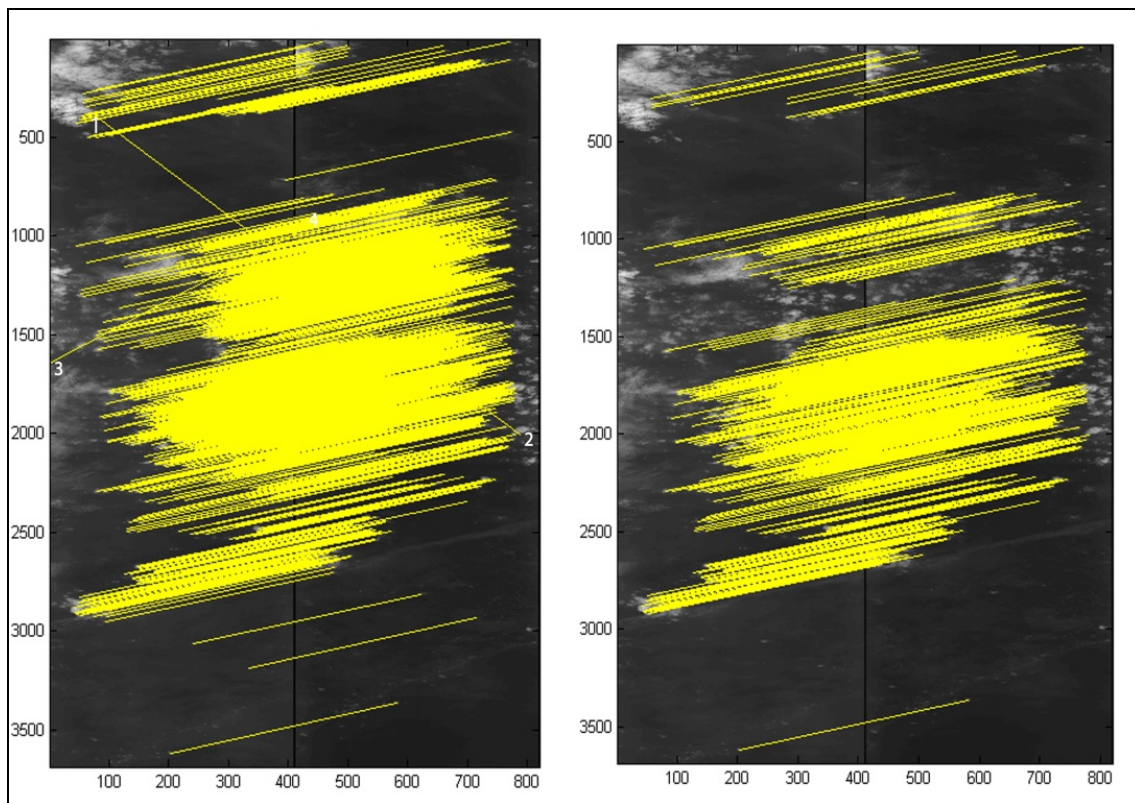
Fig. 3   Applying SIFT and SAD algorithms on G and R images: (a) applying SIFT between G and R; (b) applying SIFT and SAD between G and R.

Table 1   Applying SIFT and SAD on G-R bands.

Experiment No.	Sift CPs of reference image (green)	Sift CPs of sensed image (red)	Matched CP No.	Frame size	Threshold (Tf)	SAD CPs No.	Number of removed false SIFT CPs
1	2,554	2,186	1,485	3 × 3	200	788	697
2	2,554	2,186	1,485	3 × 3	250	533	952
3	2,554	2,186	1,485	5 × 5	250	82	1,403

Table 2   Applying SIFT and SAD on G-B bands.

Experiment No.	Sift CPs of reference image (green)	Sift CPs of sensed image (blue)	Matched CP No.	Frame size	Threshold (Tf)	SAD CP No.	Number of removed false SIFT CPs
1	2,554	678	433	3 × 3	200	193	240
2	2,554	678	433	3 × 3	250	228	205
3	2,554	678	433	5 × 5	250	73	360

Table 3   Applying SIFT and SAD on G-NIR.

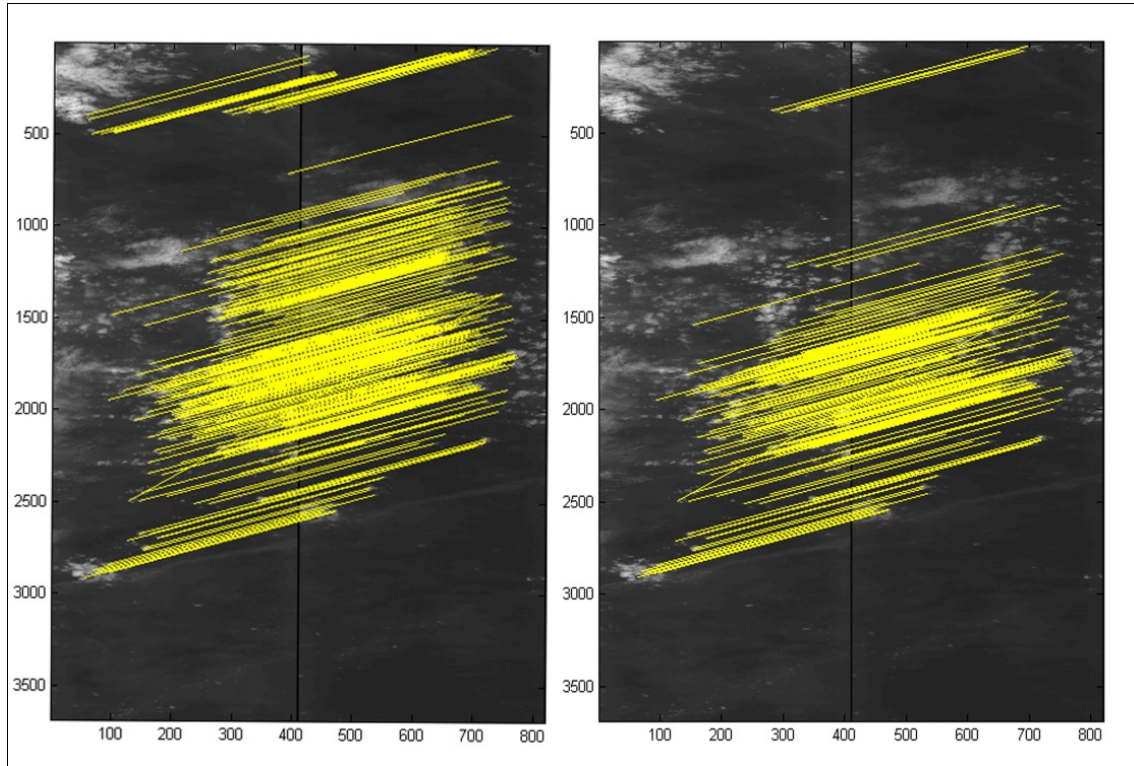| Experiment No.	Sift CPs of reference image (green)	Sift CPs of sensed image (near-infrared)	Matched CP No.	Frame size	Threshold (Tf)	SAD CP No.	Number of removed false SIFT CPs
1	2,554	1,995	815	3 × 3	200	678	137
2	2,554	1,995	815	3 × 3	250	715	100
3	2,554	1,995	815	5 × 5	250	575	240

Fig. 4   Applying SIFT and SAD algorithms on G and B images: (a) applying SIFT between G and B; (b) applying SIFT and SAD between G and B.
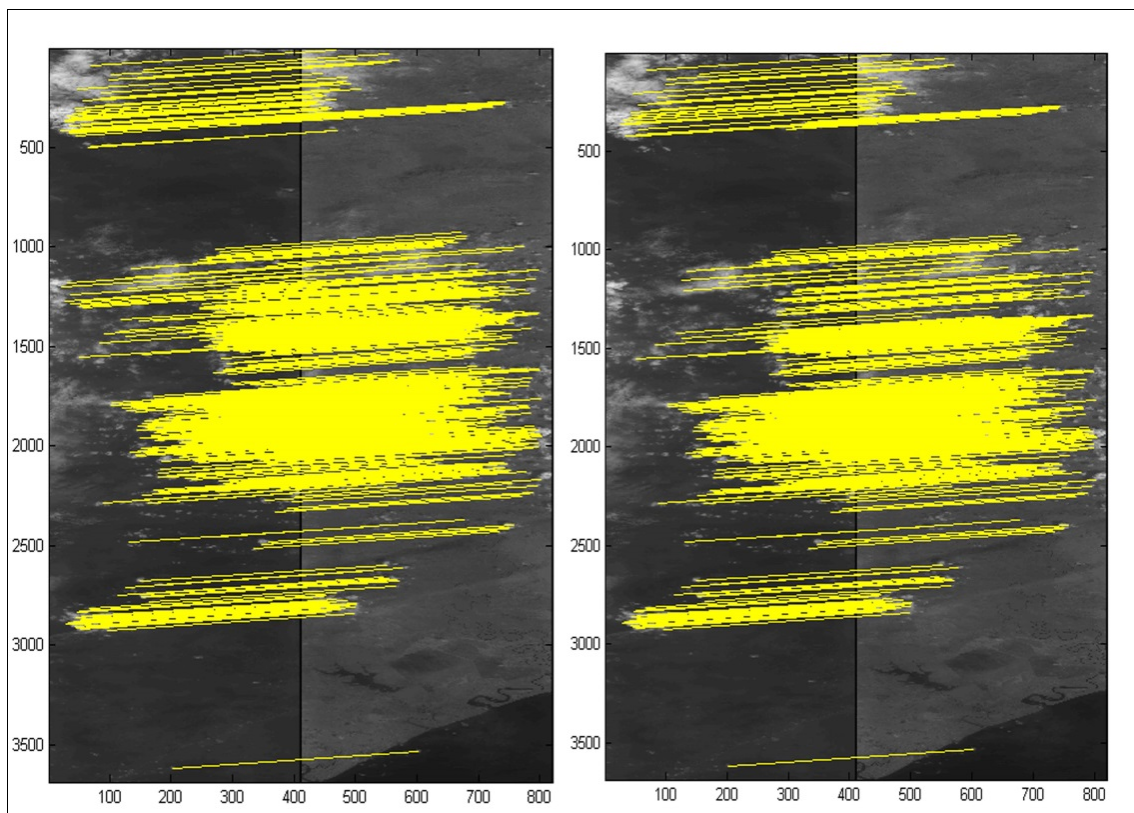

Fig. 5   Applying SIFT and SAD algorithms on G and NIR images: (a) applying SIFT between G and NIR; (b) applying SIFT and SAD between G and NIR.

Table 1 shows the operation of the SAD algorithm with different threshold values and frame sizes by applying three experiments on the reference image (green band) and slave images (red band). First, the SAD algorithm used a threshold value equal to 200 with frame size of 3 × 3. The number of extracted SIFT CPs was 2,554 and 2,186 key points in the reference and slave images, respectively, and the matched CPs were 1,485. However, after the SIFT CPs were applied to SAD, the matched CPs decreased to 788. The falsely matched CPs could not be removed by using this frame size and threshold. Thus, they still showed matching errors. In the second experiment, the threshold value was changed to 250 with the same frame size (3 × 3). The false CPs were removed, and the most accurate matched CPs were obtained by using both the SIFT and SAD algorithms. These key points represented the most accurate SIFT CPs. In the third experiment, the frame size was changed to 5 × 5, and a similar threshold value was used. Eighty-two matched CPs were obtained. The experimental results indicated that using the threshold value of 250 and frame size of 3 × 3 provides a good number of CPs and obtains the most precise matched CPs, and the bad CPs are removed from the slave and reference image. The false SIFT CPs were 952 between the reference and slave images, as shown in Table 1.

Fig. 3a shows the result of applying the SIFT algorithm, and the false CPs obviously showed matching errors. Fig. 3b presents the result of applying the SAD algorithm to the extracted SIFT CPs before the biased CPs were removed. Clearly, using the SAD algorithm based on the extracted feature showed better performance than using it based on area correlation. Moreover, Figs. 4 and 5, Tables 2 and 3 show that the matched SIFT CPs between the green and blue images (bands) were 433 and those between the green and infrared images (bands) were 815. After applying SAD with the empirical threshold equal to 250 and frame size equal to 3 × 3, the false

SIFT CPs were removed, and the refined CPs between the green and blue images (bands) and between the green and infrared images (bands) were 228 and 715, respectively. The removed and false SIFT CPs between the green and red, blue, and infrared images (bands) were 952, 205, and 100, respectively. Figs. 4 and 5 illustrate the application of SIFT and SAD algorithms between the green and red and near-infrared bands. When the results of the proposed R-SIFT method are compared with those of the original SIFT, the R-SIFT selects the true and accurate matched CPs based on the experimental results. Moreover, manually collecting the CPs is difficult and time consuming, particularly when the amount of data is large [12]. Thus, the R-SIFT is more reliable, flexible, and accurate in extracting and improving CPs. To evaluate the computational complexity of R-SIFT, the memory size and run time needed were recorded before applying R-SIFT 600 MB and two days respectively, while using the R-SIFT the memory and run time needed became 14 MB and two minutes, respectively. These results reflect that there is a significant improving in the computational efficiency by using our method.

4. Conclusion

The automatic approach of collecting and extracting of CPs by SIFT is not adequate for remotely sensed images, particularly for the new optical satellite generation of NEqO and multi-sensor images captured from different viewpoints, time and illumination. This paper presents the method to improve the extracted SIFT CPs. This paper presents a technical workflow that can be used for a large-scale mapping based on automatically refining of the extracted SIFT CPs, by involving the extracted CPs coordinates, the reference and sensed images in the SAD algorithm with using the empirical threshold. The application of R-SIFT was improved to remove false CPs that had matching errors. The RazakSAT satellite image was used in this study. The final part was evaluating the refined CPs

scenario by comparing the result of the original SIFT algorithm with that of the proposed method. The experimental results and analysis indicate the reliability and the effectiveness and robustness of the proposed method as well as the high precision that meets the requirements of registration, geometric, and change detection processing of near-equatorial and multi-sensor images. This result encourages further research to improve stability of SIFT CPs.

Acknowledgments

References

[1] Wang, S., You, H., and Fu, K. 2012. "BFSIFT: A Novel Method to Find Feature Matches for SAR Image Registration." *IEEE Geoscience and Remote Sensing Letters* 9 (4): 649-53.

[2] Fan, B., Huo, C., Pan, C., and Kong, Q. 2013. "Registration of Optical and SAR Satellite Images by Exploring the Spatial Relationship of the Improved SIFT." *IEEE Ggeoscience and Remote Sensing Letters* 10 (4): 657-61.

[3] Lowe, D. G. 2004. "Distinctive Image Features from Scale-Invariant Key-Points." *International Journal of Computer Vision* 60 (2): 91-110.

[4] Lowe, D. G. 1999. "Object Recognition from Local Scale-Invariant Features." Presented at International Conference on Computer Vision, Corfu, Greece.

[5] Mikolajczyk, K., and Schmid, C. 2005, "A Performance Evaluation of Local Descriptors." *IEEE Transactions Pattern Analysis and Machine Intelligence* 27 (10): 1615-30.

[6] Liu, J., and Yu, X. 2008. "Research on SAR Image Matching Technology Based on SIFT." In *Proceedings of International Archives of the Photogrammetry, Remote Sensing and Spatial Information Sciences*, 403-8.

[7] Hasab, H. A., Jawad, H. A., Dibs, H., Hussain, H. M., and Al-Ansari, N. 2020. "Evaluation of Water Quality Parameters in Marshes Zone Southern of Iraq Based on Remote Sensing and GIS Techniques." *Journal of Water Air Soil Pollution* 231 (183): 183-231.

[8] Schwind, P., Suri, S., Reinartz, P., and Siebert, A. 2010. "Applicability of the SIFT Operator to Geometric SAR Image Registration." *International Journal of Remote Sensing* 31 (8): 1959-80.

[9] Moigne, J. L., Campbell, W. J., and Cromp, R. F. 2002. "An Automated Parallel Image Registration Technique Based on the Correction of Wavelet Features." *IEEE Transactions on Geoscience and Remote Sensing* 40 (8): 1849-64.

[10] Jensen, J. R. 2005. *Introduction to Digital Image Processing: A Remote Sensing Perspective*. Pearson Prentice Hall, 239-47.

[11] Du, Q., Raksuntorn, N., Orduyilmaz, A., and Bruce, L. M. 2008. "Automatic Registration and Mosaicking for Airborne Multispectral Image Sequences." *Photogrammetric Engineering & Remote Sensing* 74 (2): 169-81.

[12] Zhe, L., and Fox, J. M. 2011. "Mapping Rubber Tree Growth in Mainland Southeast Asia Using Time-Series MODIS 250 m NDVI and Statistical Data." *Applied Geography* 32 (2): 420-32.

[13] Dibs, H., Mansor, S., Ahmad, N., and Pradhan, B. 2015. "Band-to-Band Registration Model for Near-Equatorial Earth Observation Satellite Images with the Use of Automatic Control Point Extraction." *International Journal of Remote Sensing* 36 (8): 2184-200. doi.org/10.1080/01431161.2015.1034891.

[14] Richards, J. A. 2013. *Remote Sensing Digital Image Analysis*. Springer-vertag Berlin Heidelberg.

[15] Dibs, H., Al-Janabi, A., and Gomes, C. 2017. "Easy to Use Remote Sensing and GIS Analysis for Landslide Risk Assessment." *Journal of University of Babylon for Engineering Sciences* 26 (1): 42-54.

[16] Ahmad, A. 2013. "Classification Simulation of RazakSAT Satellite." *Procedia Engineering* 53: 472-82. doi: 10.1016/j.proeng.2013.02.061.

[17] Hall, F. G., Strebel, D. E., Nickeson, J. E., and Goetz, S. J. 1991. "Radiometric Rectification: Toward a Common Radiometric Response among Multidate, Multisensor Images." *Remote Sensing of Environment* 35 (1): 11-27. doi: 10.1016/0034-4257(91)90062-B.

[18] Caprioli, M., Figorito, B., and Tarantino, E. 2003. "Radiometric Normalization of Landsat ETM+ Data for Multi-temporal Analysis." *The International Archives of the Photogrammetry, Remote Sensing and Spatial Information Sciences* 34.

[19] Chen, X., Vierling, L., and Deering, D. 2005. "A Simple and Effective Radiometric Correction Method to Improve Landscape Change Detection Across Sensors and Across Time." *Remote Sensing of Environment* 98 (1): 63-79. doi: 10.1016/j.rse.2005.05.021.

[20] Janzen, D. T., Fredeen, A. L., and Wheate, R. D. 2006. "Radiometric Correction Techniques and Accuracy Assessment for Landsat TM Data in Remote Forested Regions." *Canadian Journal of Remote Sensing* 32 (5):

330-40. doi: 10.5589/m06-028.

[21] Helmer, E. H., and Ruefenacht, B. 2007. "A Comparison of Radiometric Normalization Methods When Filling Cloud Gaps in Landsat Imagery." *Canadian Journal of Remote Sensing* 33 (4): 325-40. doi: 10.5589/m07-028.

[22] Canty, M. J., and Nielsen, A. A. 2008. "Automatic Radiometric Normalization of Multitemporal Satellite Imagery with the Iteratively Re-weighted MAD Transformation." *Remote Sensing of Environment* 112 (3): 1025-36. doi: 10.1016/j.rse.2007.07.013.

[23] Broncano, C. J., Pinilla, C., Gonzalez, R., and Castillo, A. 2010. "Relative Radiometric Normalization of Multitemporal Images." *International Journal of Interactive Multimedia and Artificial Intelligence* 1 (3): 53. doi: 10.9781/ijimai.2010.139.

[24] Bao, N., Lechne, A. M., Fletcher, A., Mellor, A., Mulligan, D., and Bai, Z. 2012. "Comparison of Relative Radiometric Normalization Methods Using Pseudo-Invariant Features for Change Detection Studies in Rural and Urban Landscapes." *Journal of Applied Remote Sensing* 6 (1): 1-18. doi: 10.1117/1.JRS.6.063578.

[25] Liu, S. H., Lin, C. W., Chen, Y. R., and Tseng, C. M. 2012. "Automatic Radiometric Normalization with Genetic Algorithms and a Kriging Model." *Computers & Geosciences* 43: 42-51. doi: 10.1016/j.cageo.2011.12.016.

[26] Afify, H., Helmy, A., and El, S. 2013. "Relative Radiometric Normalization Techniques of QuickBird Images, Case Study: Alexandria City." *Time Journals of Engineering and Physical Sciences* 1 (2): 19-27.

[27] Sadeghi, V., Ebadi, H., and Ahmadi, F. F. 2013. "A New Model for Automatic Normalization of Multitemporal Satellite Images Using Artificial Neural Network and Mathematical Methods." *Applied Mathematical Modelling* 37 (9): 6437-45. doi: 10.1016/j.apm.2013.01.006.

[28] Langner, A., Hirata, Y., Saito, H., Sokh, H., Leng, C., Pak, C., and Raši, R. 2014, "Spectral Normalization of SPOT 4 Data to Adjust for Changing Leaf Phenology within Seasonal Forests in Cambodia." *Remote Sensing of Environment* 143: 122-30. doi: 10.1016/j.rse.2013.12.012.

[29] Schmid, C., Gravircnrs, I. R., Europe, D., and Mikolajczyk, K. 2001. "Indexing Based on Scale Invariant Interest Points." In *Proceedings of ICCV 2001*, 525-31.

[30] Mikolajczyk, K., and Schmid, C. 2004. "Scale & Affine Invariant Interest Point Detectors." *International Journal of Computer Vision* 60 (1): 63-86.

[31] Helmer, S., and Lowe, D. G. 2004. "Object Class Recognition with Many Local Features." In *Proceedings of Conference on Computer Vision and Pattern Recognition Workshop*, 187.

[32] Yu, L., Zhang, D., and Holden, E. J. 2008. "A Fast and Fully Automatic Registration Approach Based on Point Features for Multi-source Remote-Sensing Images." *Computers & Geosciences* 34 (7): 838-48. doi: 10.1016/j.cageo.2007.10.005.

[33] Guang, W., Xin, W. H., and Juan, J. T. 2009. "An Algorithm of Parameters Adaptive Scale-Invariant Feature for High Precision Matching of Multi-source Remote Sensing Image." *Joint Urban Remote Sensing Event*, 1-7. doi: 10.1109/URS.2009.5137515.

[34] Hu, Q., and Ai, M. 2011. "A Scale Invariant Feature Transform Based Matching Approach to Unmanned Aerial Vehicles Image Geo-Reference with Large Rotation Angle." In *Proceedings 2011 IEEE International Conference on Spatial Data Mining and Geographical Knowledge Services*, 393.

[35] Deng, H., Wang, L., Liu, J., and Li, D. 2013. "Study on Application of Scale Invariant Feature Transform Algorithm on Automated Geometric Correction of Remote Sensing Images." *IFIP Advances in Information and Communication Technology* 393: 352-8.

[36] Ma, W., and Yang, J. 2011. "Target Detection Algorithm for Polarimetric SAR Images Using GOPCE." *IEEE CIE International Conference on Radar (Radar)*, 507-9.

[37] Chureesampant, K., and Susaki, J. 2014. "Automatic GCP Extraction of Fully." *IEEE Transactions on Geoscience and Remote Sensing* (1): 137-48. doi: 10.1109/TGRS.2012.2236890.

[38] Zhang, J., Li, G., and Zeng, Y. 2003. "The Study on Automatic and High-Precision Rectification and Registration of Multi-source Remote Sensing Imagery." *Journal of Remote Sensing* 9: 73-7.

[39] Wang, J., Di, K., and Li, R. 2005. "Evaluation and Improvement of Geo-Positioning Accuracy of IKONOS Stereo Imagery." *ASCE Journal of Surveying Engıneering* 131: 34-42.

[40] Shragai, Z., Barnea, S., Filin, S., Zalmanson, G., and Doytsher, Y. 2005. "Automatic Image Sequence Registration Based on a Linear Solution and Scale Invariant Key-Point Matching." In *Proceedings of the Second ISPRS BenCOS Workshop, Beijing, China*, 5-11.

[41] Wessel, B., Huber, M., and Roth, A. 2007. "Registration of Near Real-Time SAR Images by Image-to-Image Matching." In *Proceedings of Photogrammetric Image Analysis, Munich, Germany*, 179-84.

[42] Liu, L., Wang, Y., and Wang, Y. 2008. "SIFT Based Automatic Tie-Point Extraction for Multi-temporal SAR Images." In *Proceedings of International Workshop on Education Technology and Training Workshop Geoscience and Remote Sensing* 1: 499-503.

[43] Mahmudul, H., Pickering, M. R., and Xiuping, J. 2012. "Modified SIFT for Multi-model Remote Sensing Image Registration." In *Proceedings of Geoscience and Remote Sensing Symposium (IGARSS)*.

[44] Mukherjee, A., Velez-Reyes, M., and Roysam, B. 2009. "Interest Points for Hyperspectral Image Data." *IEEE Transactions on Geoscience and Remote Sensing* 47 (3): 748-60.

[45] Yi, Z., Zhiguo, C., and Yang, X. 2008. "Multi-spectral Remote Image Registration Based on SIFT." *Electronics Letters* 44 (2): 107-8.

[46] Chen, J., and Tian, J. 2009. "Real-Time Multi-modal Rigid Registration Based on a Novel Symmetric-SIFT Descriptor." *Progress in Natural Science* 19 (5): 643-51.

[47] Atallah, M. J. 2001. "Faster Image Template Matching in the Sum of the Absolute Value of Differences Measure." *IEEE Transactions Image Processing* 10: 659-63.

[48] Zabih, R., and Woodfill, J. 1994. "Non-parametric Local Transforms for Computing Visual Correspondence." In *Proceedings of European Conference of Computer Vision*, 151-8.

[49] Moravec, H. P. 1977. "Towards Automatic Visual Obstacle Avoidance." In *Proceedings of the International Joint Conference on Artificial Intelligence*, 584.

[50] Moravec, H. P. 1979. "Visual Mapping by a Robot Rover." In *Proceedings of the 6th International Joint Conference on Artificial Intelligence*, 598-600.

[51] Wong, A., and Clausi, D. A. 2010. "AISIR: Automated Inter-sensor/Inter-band Satellite Image Registration Using Robust Complex Wavelet Feature Representations." *Pattern Recognition Letters* 31 (10): 1160-7. doi: 10.1016/j.patrec.2009.05.016.

[52] Zheng, S., Huang, Q., Jin, L., and Wei, G. 2012. "Real-Time Extended-Field-of-View Ultrasound Based on a Standard PC." *Applied Acoustics* 73 (4): 423-32. doi: 10.1016/j.apacoust.2011.09.013.

[53] Piccinini, P., Prati, A., and Cucchiara, R. 2012. "Real-Time Object Detection and Localization with SIFT-Based Clustering." *Image and Vision Computing* 30 (8): 573-87. doi: 10.1016/j.imavis.2012.06.004.

[54] Dibs, H., and AL-Hedny, S. 2019. "Detection Wetland Dehydration Extent with Multi-temporal Remotely Sensed Data Using Remote Sensing Analysis and GIS Techniques." *International Journal of Civil Engineering and Technology* 10 (1): 143-54.

[55] Ji, S., Zhang, T., Guan, Q., and Li, J. 2013. "Nonlinear Intensity Difference Correlation for Multi-temporal Remote Sensing Images." *International Journal of Applied Earth Observation and Geoinformation* 21: 436-43. doi: 10.1016/j.jag.2012.06.009.

[56] Fonseca, L. M., and Manjunath, B. S. 1996. "Registration Techniques for Multi-sensor Remotely Sensed Imagery." *Photogrammetric Engineering and Remote Sensing* 62 (9): 1049-56.

[57] Inglada, J., and Giros, A. 2004. "On the Possibility of Automatic Multi-sensor Image Registration." *IEEE Transactions on Geoscience and Remote Sensing* 42 (10): 2104-20.

[58] Bentoutou, Y., Taleb, N., Kpalma, K., and Ronsin, J. 2005. "An Automatic Image Registration for Applications in Remote Sensing." *IEEE Transactions on Geoscience and Remote Sensing* 43 (9): 2127-37.

[59] Chureesampant, K. and J. Susaki, 2012, "Automatic unsupervised change detection using multi-temporal polarimetric SAR data," *IEEE International Geoscience and Remote Sensing Symposium (IGARSS)*, 6192–6195.

[60] Reinhard, E., Stark, M., Shirley, P., and Ferwerda, J. 2002. "Photographic Tone Reproduction for Digital Images." *ACM Transactions on Graphics* 21 (3): 267-76.

[61] Dibs, H. 2018. "Comparison of Derived Indices and Unsupervised Classification for AL-Razaza Lake Dehydration Extent Using Multi-temporal Satellite Data and Remote Sensing Analysis." *Journal of Engineering and Applied Sciences* 13 (24): 1-8.

[62] Dandekar, O., and Shekhar, R. 2007. "FPGA-Accelerated Deformable Image Registration for Improved Target-Delineation during CT-Guided Interventions." *IEEE Transactions on Biomedical Circuits and Systems* 1: 116-27.

[63] Cheng, L., Gong, J., Yang, X., Fan, C., and Han, P. 2008. "Robust Affine Invariant Feature Extraction for Image Matching." *IEEE Geoscience and Remote Sensing Letters* 5 (2): 246-50.

[64] Mitterberger, M., Christian, G., Pinggera, G. M., Bartsch, G., Strasser, H., and Pallwein, L. 2007. "Gray Scale and Color Doppler Sonography with Extended Field of View Technique for the Diagnostic Evaluation of Anterior Urethral Strictures." *Journal of Urology* 177: 992-6.

[65] Watman, C., Austin, D., Barnes, N., Overett, G., and Thompson, S. 2004. "Fast Sum of Absolute Differences Visual Landmark Detector." In *Proceedings of IEEE International Conference on Robotics and Automation (ICRA 2004)*, 4827-32.